Trans. Inst. Indian Geographers
ISSN 0970-9851
Indexed in Scopus

Assessment of the spatio-temporal interaction between land use transformation, land surface temperature, and land cover environment- A case study of Chennai Metropolitan Area, India

Manikandan N.*, Dharshan Shylesh D. S., Jaganathan R., Tamilnadu; Mahalingam B., Karnataka; Sivasankar S., Sangunathan U., and Manivel P., Tamilnadu

Abstract

This study investigates land use changes that influence the land surface temperature (LST) of the land cover environment in the Chennai Metropolitan Area (CMA), India, over three decades (1991-2021). Landsat satellite imageries were used to classify the CMA into six land use and land cover (LULC) types using the Support Vector Machine (SVM) classification technique. Similarly, LST was calculated using Thermal Infrared (TIR) bands through the conversion of radiation into temperature and estimated emissivity (e) through Normalized Difference Vegetation Index (NDVI) calculation. The result shows that LST increased from 35.6°C to 47.2°C. To evaluate the relationship between LST and LULC over the study period, Zonal Statistics Analysis (ZSA) was used. The findings show a steady rise in LST across all types of land use and land cover, with a built-up area-specific trend being particularly notable. The linear correlation between the mean sensitive land use and land cover (LULC) and the mean land surface temperature (LST) shows a strong positive relationship between the mean LST and the mean Normalized Difference Built-Up Index (NDBI). These findings highlight the significant influence of land use changes, particularly built-up land, on the increasing LST of the surrounding land cover.

Keywords: *Land Surface Temperature (LST), Support Vector Machine (SVM), Thermal infrared (TIR), Zonal Statistics Analysis (ZSA), Normalized Difference Built-Up Index (NDBI).*

Introduction

The rapid expansion of impervious surfaces in urban areas has a significant environmental impact, leading to changes in surface properties and contributing to the urban heat island (UHI) effect. Several megacities in India are experiencing significant horizontal and vertical development. This study aims to investigate the complex relationship between land use changes, land surface temperature (LST), and the overall land cover environment in the Chennai Metropolitan City.

Understanding the intricate relationship between land use transformation, LST, and the land cover environment in the Chennai metropolitan city is crucial for informed urban planning and effective

adaptation to climate change. This study provides comprehensive insights into how urbanization influences temperature patterns and environmental conditions with its implications for sustainable development. The global significance of studying land use and land cover (LULC) changes and their impact on LST is evident in the substantial attention this subject has received from researchers worldwide. Numerous studies, employing diverse methodologies, have demonstrated a significant association between land use dynamics and LST variations. For instance, Saha *et al.* (2020) conducted a comprehensive study in Kolkata using Landsat data spanning over 1988 to 2018, revealing a notable correlation between land use changes and LST. Similarly, Das *et al.* (2022) identified a substantial increase in seasonal LST in Chandannagar city, Kolkata, attributed to LULC changes. Chanu *et al.* (2021) observed significant LULC changes in the Greater Chennai region over 11 years, with a noteworthy temperature increase from 37.61°C in 2005 to 41.25°C in 2016. Exploring LST in major Indian metro cities, Shahfahad *et al.* (2020) utilized advanced algorithms like a mono window (MWA) and split window (SWA), correlating their findings with NDVI and NDBI. Mumbai exhibited the highest LST, while Kolkata recorded the lowest, showcasing diverse accuracy in coastal and interior cities between MWA and SWA. Chatterjee *et al.* (2021) delved into LULC and LST changes in Kolkata from 2005 to 2019, revealing reduced vegetation cover towards the city core and urban expansion towards the outskirts, resulting in a peak LST of 41°C in 2019. In the South Karkheh Sub-basin, Iran, Ghobadi *et al.* (2013) unveiled a negative correlation between LST and NDVI, affirming vegetation's cooling effect. Examining four Nigerian cities, Ayanlade *et al.* (2021) linked LST increases to changes in LULC, emphasizing the urban heat island effect. Similarly, Kesavan *et al.* (2021) identified higher LST in four Nigerian cities due to LULC changes, using the ARIMA model to reveal a progressive increase in LST in built-up areas.

Previous studies extensively explored the relationship between land use changes and Land Surface Temperature (LST), utilizing remote sensing data, GIS techniques, statistical analysis, and predictive modelling. However, this study distinguishes itself by specifically investigating the influence of land-use changes on variations in LST and their subsequent impact on the temperatures of the surrounding land cover. Chennai Metropolitan Area (CMA), the capital of Tamil Nadu, has undergone rapid growth, leading to extensive infrastructure development and a substantial increase in its geographical extent. According to the 2022 report by the Chennai Metropolitan Development Authority, the CMA has expanded from 1189 km^2 to 5904 km^2. This expansion has resulted in the loss of natural landscapes, disruption of ecosystems, and alterations in hydrological patterns (Anushiya *et al.*, 2021). The present study provides valuable and reliable insights into the environmental conditions of the rapidly urbanizing CMA, offering relevance for understanding similar trends in other highly urbanized regions. The research identifies heat stress areas, aids urban comfort, and supports biodiversity preservation. This study aims to (1) examine LULC and LST changes, (2) explore the influence of land use changes on LST and land cover, and (3) determine the impact of mean LST on sensitive categories.

Study area

Situated in southern India, the CMA is a large metropolis covering 1,189 km^2 and positioned between latitudes 12°50'49"N and 13°17'24"N, and longitudes 79°59'53"E and 80°20'12"E (Fig. 1). Experiencing a tropical wet and dry climate due to its coastal proximity and the thermal equator, the CMA experiences scorching temperatures in May and June (35°C–40°C), while January represents the coldest period with temperatures around 19–25°C.

The city receives an average annual rainfall of approximately 1400 mm, with the highest during the Northeast monsoon season (October to December) (IMD 2010). Chennai has evolved into a thriving information technology hub, transitioning from its commercial and manufacturing origins (Krishnamurthy and Desouza, 2015) which are responsible for attracting a larger population to the Chennai Metropolitan Area (CMA). Additionally, the CMA benefits from a well-established transportation network that efficiently connects it to major cities across India. Its flat terrain and coastal position along the Bay of Bengal further contribute to its position as one of the most densely populated regions in the country. According to the 2011 census, Chennai's urban agglomeration accommodated around 8.65 million people, resulting in a population density of 2,109 persons per km^2.

Dataset

Satellite data from Landsat 5 TM, 7 ETM+, and 8 OLI/TIRS sensors were obtained for 1991, 2001, 2011, and 2021 from the USGS website (Table 1). Images closest to the vernal or autumnal equinox were prioritized for equal radiation, enhancing reliability for LST and LULC estimation. The acquired images correspond to Row 142 and Path 051 in the WRS, projected using the WGS 84 datum and UTM coordinate system (Zone 44 North). Pre-processing involves multiple steps. Layer stacking combined the Blue, Green, Red, and NIR bands, followed by histogram equalization to enhance contrast in all bands. The LULC classification was performed using the stacked images, and ancillary data from sources such as the Survey of India (SOI) Toposheet (1: 50,000 scale) and Google Earth images were used to create training data for classification and evaluate result accuracy. For land surface temperature calculations, Thermal Infrared Sensor (TIRS) Band 6 was employed for Landsat-5 and Landsat-7, while Band 10 was used for Landsat-8. Normalized Difference Vegetation Index (NDVI) computation utilized the Near Infrared (NIR) and Red bands. Similarly, Short Wave Infrared (SWIR) and NIR bands were employed for the Normalized Difference Built-Up Index (NDBI) calculation, and Green and Red bands were used for the Normalized Difference Water Index (NDWI).

Methods

SVM classification

For Land Use and Land Cover (LULC) classification, the study employed Support Vector Machine (SVM) algorithms through the ENVI 5.2 image processing software. Introduced by Vapnik in 1995, SVM has gained widespread acceptance in remote sensing due to its robust statistical basis and superior empirical performance. It outperforms traditional techniques such as neural networks and maximum likelihood classifiers, as evidenced by various studies (Singh *et al.*, 2014). Foody & Mathur (2004) demonstrated SVM's higher accuracy in

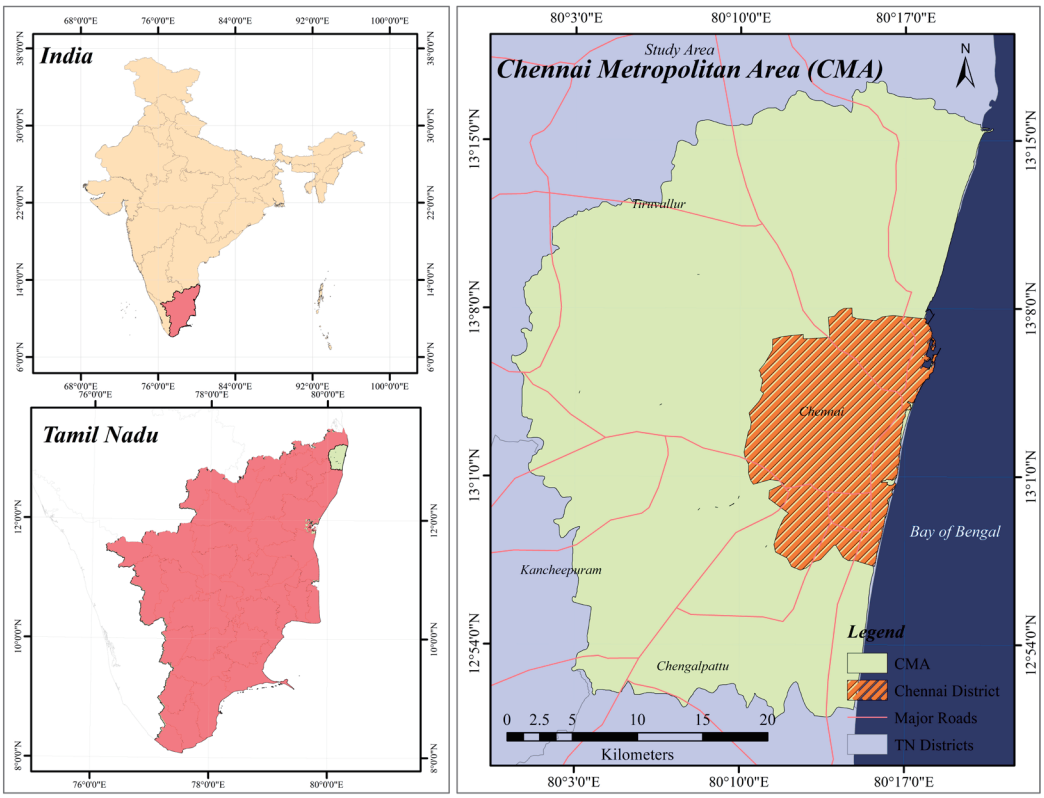

Fig. 1 Study area

Table 1: Satellite data specifications

Date	Landsat/Sensor	Scene ID
26.09.1991	5 TM	19910926_20170126_01_T1
21.03.2001	7 ETM +	20010321_20170206_01_T1
09.03.2011	5 TM	20110309_20161209_01_T1
20.03.2021	8 OLI/TIRS	20210320_20210328_02_T1

multi-class image classification compared to classifiers like discriminant analysis (DA), decision tree (DT), and feed-forward neural network. The SVM classification utilized four kernels: linear, polynomial, Radial Basis Function (RBF), and sigmoid. The study specifically applied the RBF kernel due to its low computational complexity and effectiveness in handling non-linear relationships between training data and the entire dataset, as recommended by Mishra *et al.* (2019). The RBF kernel function is represented in Equation 1.

$$K(x_i, x_j) = exp(-\gamma || (x_i - x_j) ||^2), \gamma > 0 \quad \text{(Eq. 1)}$$

Using Anderson's classification (1976) and NRSC's 2012 categorization, CMA was classified into six types of LULC: fallow

land, built-up land, vegetation, scrubland, and water bodies. Following the pre-processing of satellite images, training data were collected for each land use and land cover class from the satellite imagery, aided by Survey of India toposheets and Google Earth. These selected samples were then used as input for SVM classification.

Accuracy assessment

Correctness refers to the extent of alignment between classified satellite images and the actual ground truth. This assessment method gauges how accurately the classified map represents the real land cover and land use on the ground, utilizing reliable reference data such as GPS data, ground truth data, and high-resolution imagery. To evaluate categorization accuracy, a total of 288 checkpoints were randomly selected through a robust sampling procedure. Various measures, including overall classification accuracy, producer accuracy, user accuracy, and Cohen's Kappa coefficient (1960), were calculated (Eq. 2).

$$K = \frac{N\sum_{i=1}^{r} x_{ii} - \sum_{i=1}^{r} (x_{i+})(x_{+i})}{N^2 - \sum_{i=1}^{r} (x_{i+})(x_{+i})} \qquad \text{(Eq. 2)}$$

In the matrix, 'r' denotes the number of rows, and 'xii' signifies the count of observations in both column 'i' and row 'i' (diagonal elements). 'x+i' and 'xi+' represent the marginal totals in row 'r' and column 'i,' respectively, while 'N' stands for the total number of observations. User accuracy metrics and producer accuracy metrics, addressing commissions and omissions, have been thoroughly discussed by Singh, P. (2018). Subsequent to calculating the area and changes in LULC, the LST was computed using specific steps.

Retrieval of land surface temperature (RLST)

Conversion of digital numbers to sensor radiance: The TIRS bands recorded by Landsat sensors are stored as digital numbers (DN), representing various brightness levels. The first step in calculating LST is the conversion of DN values to radiance. Specifically, for Landsat-8, the DN is transformed into spectral radiance (Eq. 3).

$$L_\lambda = M_L * Q_{cal} + A_L - O_i \qquad \text{(Eq. 3)}$$

In the equation, Lλ represents spectral radiance (W m-2 sr-1 µm-1), ML and AL are rescaling factors, Qcal denotes quantized and calibrated pixel value (DN), and Oi represents the calibration offset. For Landsat-8 TIRS band 10, the calibration factor is 0.29 (usgs. gov 2016). DN was converted to radiance in Landsat-5 TM and Landsat-7 ETM+ using a spectral radiance rescaling equation (Eq. 4), which differed from Landsat-8.

$$L_\lambda = \left(\frac{LMAX_\lambda - LMIN_\lambda}{Q_{calmax} - Q_{calmin}}\right)(Q_{cal} - Q_{calmin}) + LMIN_\lambda \qquad \text{(Eq. 4)}$$

In the context of calculating LST, Lλ is the spectral radiance at the sensor (measured in W m-2 sr−1 µm−1). LMAXλ is the spectral radiance scaled to the maximum quantized calibrated pixel value (Qcalmax), and LMINλ is the spectral radiance scaled to the minimum quantized calibrated pixel value (Qcalmin), both measured in W m-2 sr−1 µm−1. Qcalmin corresponds to the minimum quantized calibrated pixel value, and Qcalmax corresponds to the maximum value. All variables, except for Qcal, are provided in the metadata file of a scene.

Computation of brightness temperature

After converting DN to radiance, the next step is to apply Eq. 5 to convert radiance to brightness temperature. This concept is based

Table 2: NDVI and emissivity threshold levels

NDVI value	Land surface emissivity
NDVI < - 0.185	0.995
-0.185 <NDVI < 0.157	0.970
0.157 < NDVI < 0.727	1.0094 + 0.047 * ln (NDVI)
NDVI > 0.727	0.990

on the idea that a black body must reach a certain brightness temperature to emit or receive an equal amount of radiation per unit surface area.

$$T_{sen} = \frac{K_2}{\ln\left(\frac{K_1}{L_\lambda}+1\right)} - 273.15 \qquad \text{(Eq. 5)}$$

Tsen represents the top of atmosphere brightness temperature, while Lλ denotes the top of atmosphere spectral radiance (Watts m-2 srad-1 μm−1). K1 and K2 are band-specific thermal conversion constants obtained from the metadata. The resulting values were then converted from Kelvin to Celsius.

Determination of land surface emissivity (LSE)

The NDVI, derived from the reflectance of Earth's features in the NIR and Red bands of the electromagnetic spectrum, is utilized to calculate emissivity (ε) and vegetation proportion (Pv) for determining LST. Positive NDVI values indicate vegetated areas, while negative values show non-vegetated surfaces. For Landsat-5 TM and Landsat-7 ETM+, band 3 is red, and band 4 is NIR. For Landsat 8 OLI/TIRS, band 4 is red, and band 5 is NIR (Eq. 6).

$$NDVI = \frac{NIR - Red}{\text{NIR} + \text{Red}} \qquad \text{(Eq. 6)}$$

Calculation of surface emissivity using the NDVI threshold method

Surface emissivity, a crucial factor in LST inversion, accounts for the variance in heat radiation emitted by different LULC types. Emissivity (ε) is defined as the ratio of radiated light to blackbody emission at a given wavelength and temperature. The NDVI threshold approach was employed to calculate surface-specific emissivity, relying on the strong linear correlation between NDVI and particular surface emissivity. The NDVI threshold approach (Table 2) was utilized for emissivity calculation.

Calculation of land surface temperature

The Landsat series data has been utilized to calculate the LST for each pixel (Eq. 7), where BT is the brightness temperature, λ is the wavelength of the radiance emitted in each band, σ is the Stefan-Boltzmann constant, and ε is the surface emissivity.

$$LST = \left[BT/\left(1 + \lambda * \frac{BT}{\rho * \ln(\varepsilon)}\right)\right] \qquad \text{(Eq. 7)}$$

Zonal statistics (ZA)

Zonal Statistics is a tool employed for calculating statistics within specified zones in a dataset, offering insights into spatial patterns and relationships. It facilitates the analysis of variables like land cover, temperature, and other geospatial data within defined zones, allowing users to comprehend patterns and make informed decisions. Zonal-based spatial analysis provides a collection of more micro-sized observations (Openshaw, 1996). A single output value is generated for each zone in the input zone dataset, revealing

Table 3: Accuracy assessment for the years 1991, 2001, 2011, and 2021.

Class Name	1991		2001		2011		2021	
	Producers Accuracy (%)	Users Accuracy (%)	Producer Accuracy (%)	User Accuracy (%)	Producer Accuracy (%)	User Accuracy (%)	Producer Accuracy (%)	User Accuracy (%)
Water bodies	93.33	93.33	92.86	86.67	100.00	92.86	87.50	87.50
Built-up	94.74	81.82	97.73	87.76	90.38	90.38	100.00	95.40
Fallow land	94.44	86.08	92.31	92.31	87.93	89.47	89.47	91.89
Vegetation	47.83	84.62	61.54	80.00	75.00	85.71	25.00	100.00
Scrubs	50.00	100.00	20.00	100.00	33.33	100.0	72.73	100.00
Agriculture	88.24	78.95	85.71	75.00	100.00	84.62	100.00	82.35
Classification accuracy	86.06		88.82		89.02		93.04	
Kappa statistics	0.8063		0.8323		0.8517		0.891	

the association between LULC and LST. This approach proves effective in evaluating the relationship between LULC and LCT (Ghobadi *et al*., 2013). The Zonal Statistics results offer valuable insights into the actual trends of LST within each LULC type and how the LST of land cover features is influenced by the surrounding land use. Such analysis contributes to a deeper understanding of the thermal behaviour of various land cover elements, shedding light on the dynamics and interactions between land use and LST across the research period.

Results and discussion

Accuracy assessment

Table 3 summarizes LULC categorization accuracy, producer accuracy, and user accuracy. Water bodies consistently exhibit high accuracy, with producer accuracy ranging from 92.86 to 100 percent, and user accuracy from 86.67 to 92.86 percent, indicating reliable classification throughout the year. Built-up areas also demonstrate high accuracy, with producer accuracy ranging from 87.76 to 100 percent and user accuracy from 81.82 to 95.40 percent. Fallow Land maintains consistent accuracy, with producer accuracy between 87.93 and 94.44 percent, and user accuracy from 86.08 to 92.31 percent. Vegetation accuracy varies, with producer accuracy between 47.83 and 85.71 percent, and user accuracy from 61.54 to 100 percent, notably improving between 2011 and 2021. Scrubland accuracy ranges from 33.33 to 100 percent, with producer accuracy from 33.33 to 100 percent, and user accuracy from 20 to 100 percent, showing improvement between 2011 and 2021.

The accuracy of agricultural land is consistent, with producer accuracy ranging from 78.95 to 100 percent, and user accuracy from 75 to 88.24 percent.

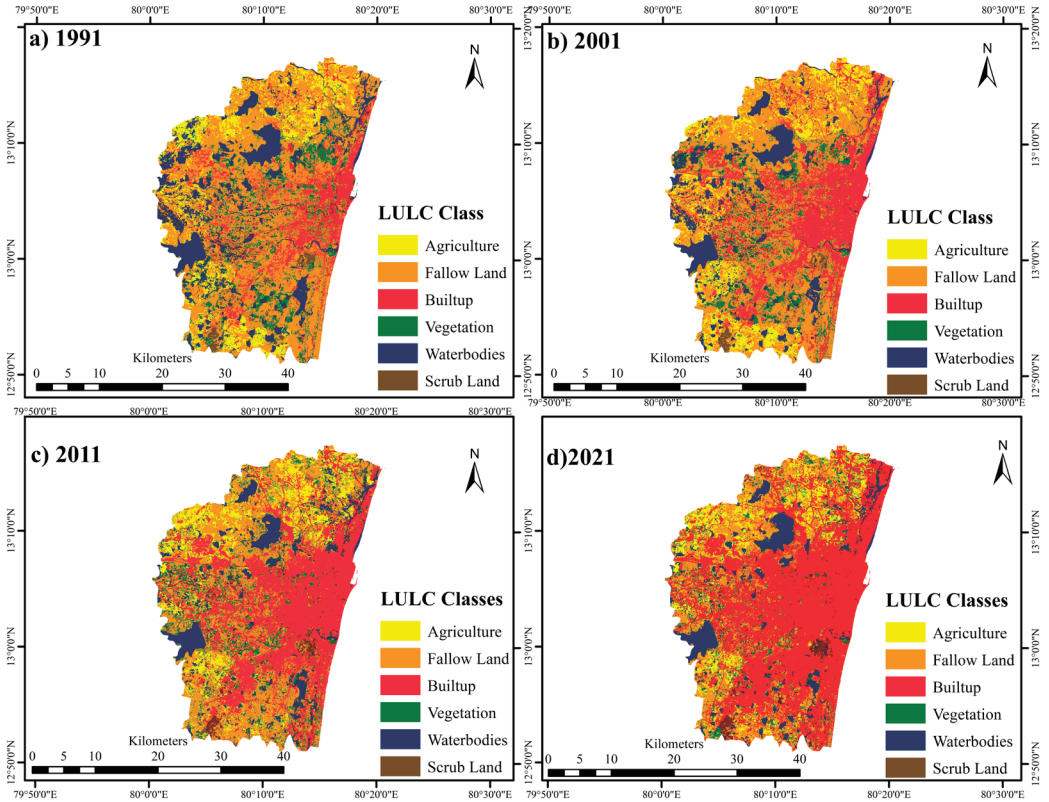

Fig. 2: Land Use and Land Cover map a) 1991 b) 2001 c) 2011 and d) 2021

Table 4: Area Calculation of LULC

Class Name	Area in (km^2)				Area (%)			
	1991	2001	2011	2021	1991	2001	2011	2021
Agriculture	122.5	122.7	140.6	123.6	10.3	10.3	11.8	10.4
Fallow Land	589.5	534.7	400.6	252.2	49.6	45	33.7	21.2
Built-up	144.8	277.4	395.3	620.3	12.2	23.3	33.3	52.2
Scrubs	18	17.4	14.5	16.4	1.5	1.5	1.2	1.4
Vegetation	118.3	91.7	105.5	61.8	10	7.7	8.9	5.2
Water bodies	195.2	144.5	131.8	114	16.4	12.2	11.1	9.6
Total	1188.4				100			

Overall classification accuracy ranges from 86.06 to 93.04 percent, indicating an increasing trend over time. The categorization of kappa in this study varies from 0.81 to 0.891, falling within an acceptable range.

Land use and land cover area

Table 4 and Fig. 2 represent the areas of different LULC classes in square kilometres and their corresponding percentages for 1991,

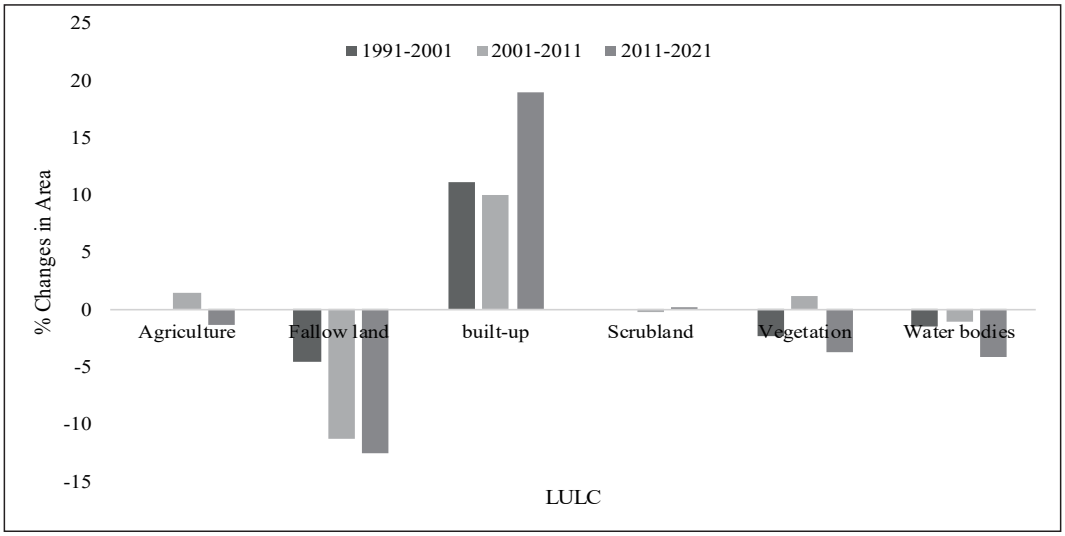

Fig. 3: Dynamics of LULC, 1991-2021

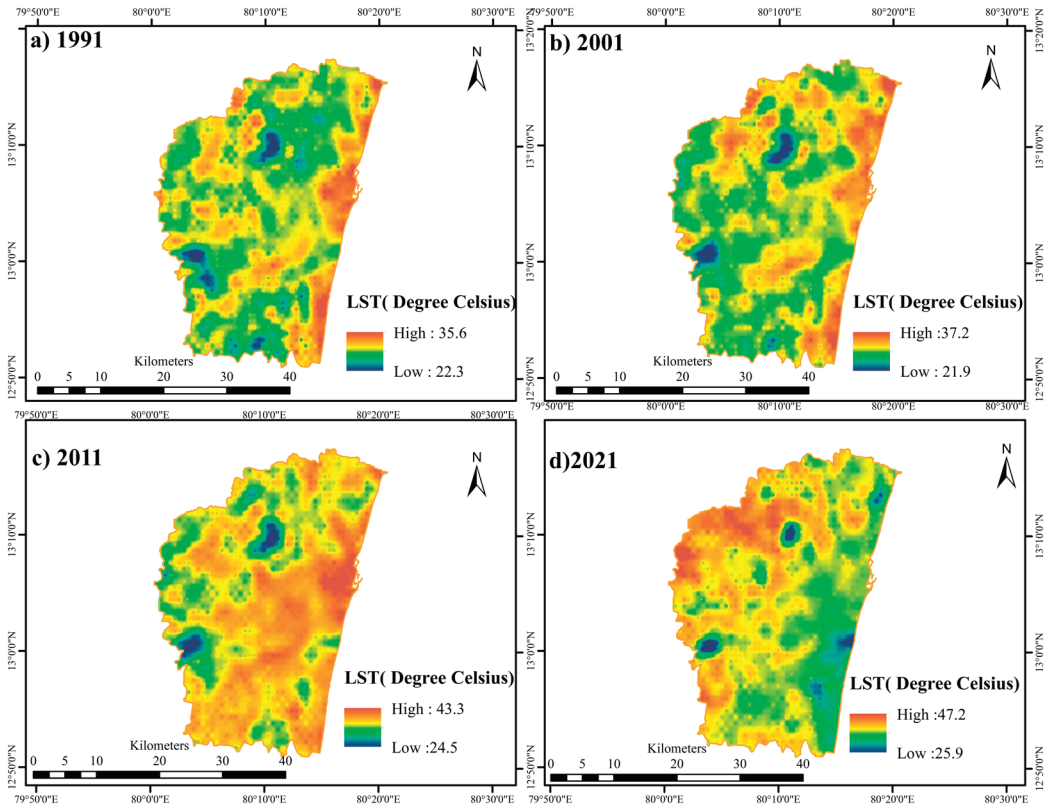

Fig. 4: Land Surface Temperature a) 1991 b) 2001 c) 2011 d) 2021

Table 5: LULC changes

Class	Changes in km^2			Changes in Percentage		
	1991-2001	2001-2011	2011-2021	1991-2001	2001-2011	2011-2021
Agriculture	0	17.9	-17	0	1.5	-1.4
Fallow land	-4.6	-134.1	-148.4	-4.6	-11.3	-12.5
built-up	11.1	117.9	225	11.1	10	18.9
Scrubland	0	-2.9	1.9	0	-0.3	0.2
Vegetation	-2.3	13.8	-43.7	-2.3	1.2	-3.7
Water bodies	-17.8	-12.7	-4.2	-1.5	-1.1	-4.2

Table 6: LST statistics from 1991 – 2021

Year	Land surface Temperature			
	Maximum	Minimum	Mean	STD
1991	35.6	22.3	28.95	1.89
2001	37.2	21.9	28.15	1.81
2011	43.3	24.5	32.63	2.63

2001, 2011, and 2021 (Fig. 2).

The agricultural land area has slightly decreased, potentially due to its concentration in the outer peripheral regions. A notable transformation is evident, where a significant portion of fallow land has been converted into built-up areas. Figures 2(a) to 2(d) illustrate the CMA's expansion in built-up areas, particularly in the southern and western directions with Chennai as the focal centre. Figure 2(a) shows sparsely developed territory in the southern and western directions, which has expanded in all directions over time, contributing to the observed built-up land cover in 2021. In 2021, there was a substantial increase in built-up land to approximately 620.3 km^2, while fallow land decreased to 252.2 km^2, indicating ongoing urbanization or development in the region. The expanded built-up land has encroached upon smaller-sized water bodies, especially in the central part of CMA.

The most striking trend revealed by Table 5 and Figure 3 is the consistent increase in built-up areas over the three decades, with a significant rise of 225 km^2 from 2011 to 2021. This points to rapid urbanization and expansion of impervious surfaces within the study area. Conversely, fallow land experienced substantial decreases, notably declining by 148.4 km^2 from 2011 to 2021. This suggests a significant shift away from fallow land use. These contrasting trends highlight the dominant impact of urban development on land cover changes.

Land surface temperature

From 1991 to 2021, the CMA exhibited a consistent increase in LST (Table 6 and Figure 4). The mean temperature rose steadily from 28.95°C in 1991 to 37.49°C in 2021. The standard deviation also increased significantly from 1.89°C in 1991 to 2.43°C in 2021, highlighting growing unpredictability. These trends emphasize the presence of

Table 7: Zonal statistical analysis (ZSA) of LULC and LST

Year	Statistic	Land Use			Land Cover Temperature		
		Built-up	Fallow land	Agriculture	Water bodies	Scrubland	Vegetation
1991	Min	22.39	22.39	22.38	22.82	22.82	22.82
	Max	35.68	35.29	32.93	35.29	34.09	35.68
	Mean	28.78	28.48	26.93	26.17	27.16	27.22
	SD	1.45	1.57	1.67	1.94	1.74	1.58
2001	Min	23.69	23.25	24.12	21.95	23.26	22.85
	Max	37.26	36.47	33.69	35.68	34.89	34.89
	Mean	28.81	28.83	27.38	25.76	26.7	27.41
	SD	1.48	1.56	1.35	1.28	1.17	1.34
2011	Min	25	25	24.5	25	25.4	25
	Max	43.4	42.6	41.9	42.6	39.3	41.9
	Mean	33.9	33	31.5	29.4	31.9	32.2
	SD	1.8	2.1	2.3	3.2	1.8	2.3
2021	Min	25.99	28.2	28.58	27.22	29.02	28.96
	Max	47.06	47.17	46.22	47.23	45.79	46.53
	Mean	37.28	38.54	38.41	35.73	35.82	37.26
		1.85	2.05	2.4	4.08	1.75	2.44

urban heat island effects and the need to address the impact of rising LST on the urban environment and human health in CMA.

Zonal statistics

Zonal statistics over three decades reveal significant temperature changes across different land cover classes (Table 7). Maximum Land Surface Temperature (LST) steadily rose in Built-up areas, from 35.68°C in 1991 to 47.06°C in 2021, indicating consistent warming. Similarly, LST increased in fallow land (35.29°C to 47.17°C) and agriculture (32.93°C to 46.22°C) over the same period, suggesting overall warming trends. Notably, the mean LST of Built-up areas showed a significant upward trend. While fallow land remained relatively stable, agriculture exhibited a clear increase. Moreover, temperature variability within the study area saw moderate changes in Built-up areas and a notable increase in agriculture over the years.

Water bodies, scrubland, and vegetation demonstrated notable changes in LST over the studied period. Water bodies exhibited an increase in maximum LST, suggesting warming trends, while the mean LST consistently rose. Scrubland maintained relatively stable readings, and vegetation showed a significant temperature rise. Additionally, the standard deviation of LST increased for water bodies, indicating greater temperature variability. These findings

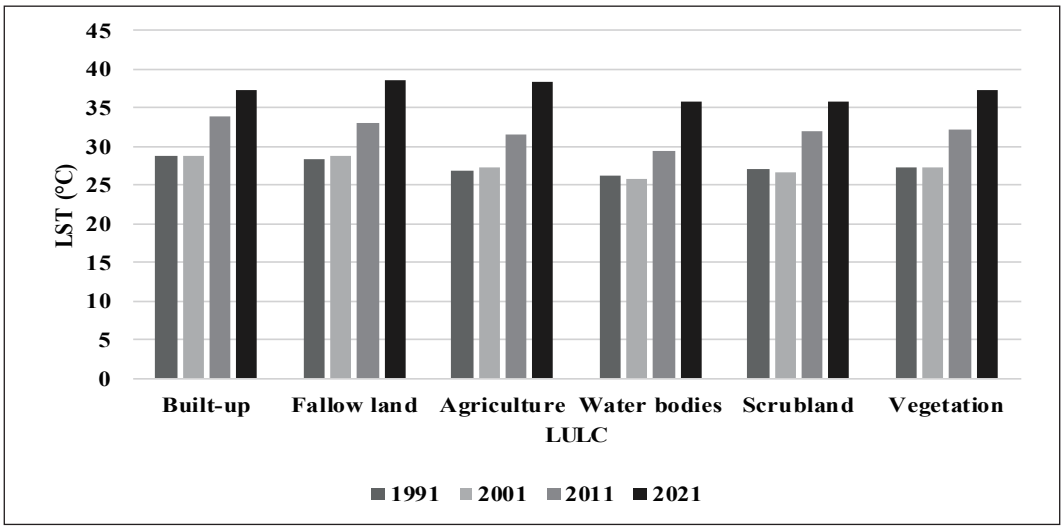

Fig. 5: Mean LST of Land use & land cover, 1991-2021

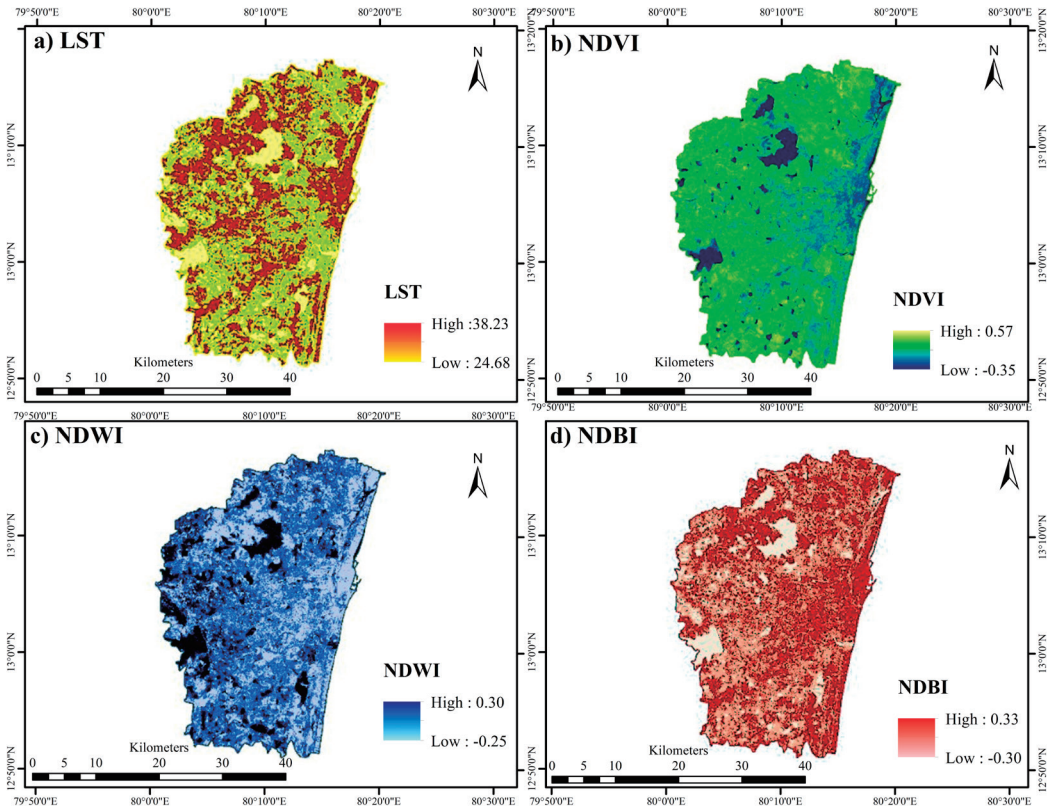

Fig. 6: Mean LST and mean LULC a) Mean LST b) Mean NDVI
c) mean NDWI d) Mean NDB1

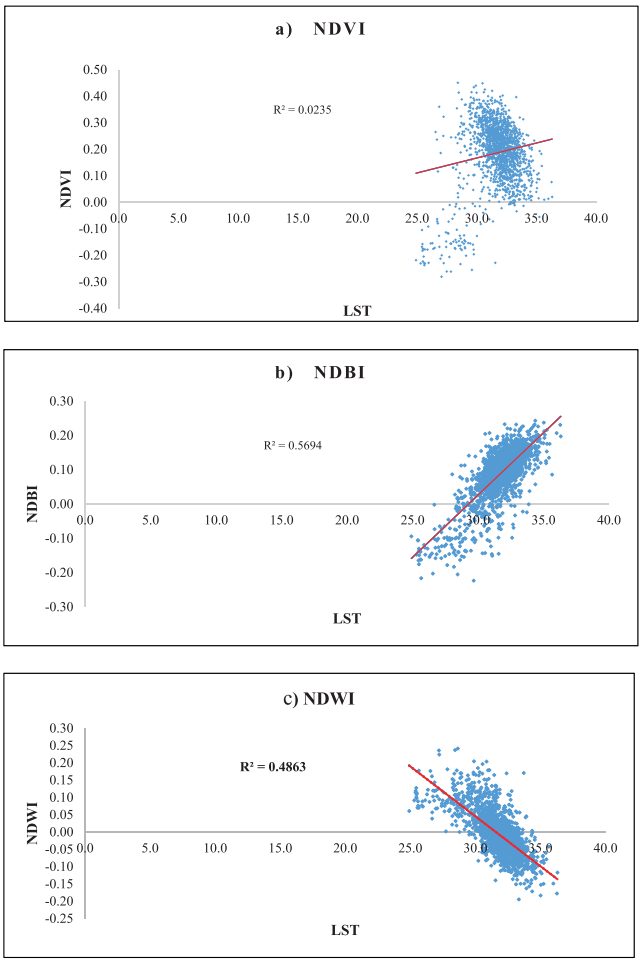

Fig. 7: Linear correlation between LST and various mean Sensible LULC
a) Mean NDVI and Mean LST, b) Mean NDWI and LST, c) Mean NDBI and Mean LST

underscore the diverse thermal behaviours of various land cover types and their potential implications for ecosystem dynamics and climate monitoring.

Relation between LST, LU, and LC Environment

The zonal statistical analysis in Figure 5 and Table 7 reveals a consistent trend of increasing surface temperatures over time in different land use and land cover types. Built-up areas, fallow land, and agriculture- all show rising LST values, indicating a warming trend. Similarly, water bodies, scrubland, and vegetation exhibit an upward trend in LST levels, with vegetation experiencing a particularly significant temperature increase. These findings highlight a potential correlation between land use and land cover types, emphasizing the distinct thermal characteristics of each category and their

potential impact on ecosystem dynamics and climate monitoring. Further research could explore a finer-grained linear correlation between land use LST and land cover LST to strengthen this connection.

Correlation between LST & sensible LU and LC

Statistical analysis is performed to establish a linear relationship between different spectral indices, including the mean Normalized Difference Built-up Index (NDBI), Normalized Difference Vegetation Index (NDVI), Normalized Difference Water Index (NDWI), and the mean Land Surface Temperature (LST) (Fig. 6).

The correlation between mean LST and NDVI is weak (R-squared = 0.0235), suggesting a minimal linear relationship. Other LULC factors may have a stronger influence on LST.

The correlation between mean LST and NDWI is moderate (R2 = 0.4863) indicating a moderate linear relationship, with NDWI explaining 48.63 percent of the LST variation. Similarly, the correlation between mean LST and NDBI is relatively strong (R2 = 0.5694), with NDBI explaining around 56.94 percent of the LST variation (Fig. 7).

Conclusion

The impact of three decades of land use changes on land surface temperature in the Chennai Metropolitan Area (1991-2021) was examined using Landsat satellite imagery and Support Vector Machine (SVM) techniques. This study reveals a significant increase in built-up land over the years, while all other land uses show decreasing trends. This indicates that urbanization is the primary driver dominating other Land Use and Land Cover (LULC) changes. Similarly, Land Surface Temperature (LST) has steadily risen from 1991 to 2021, with maximum and minimum temperatures, along with mean LST, increasing by almost 8.5 degrees Celsius over the period.

The analysis of Zonal Statistics shows that built-up areas consistently exhibit the highest mean LST compared to other LULC types. However, temperatures for all other land uses also show a gradually increasing trend over the study period. Mean LST demonstrates a moderate correlation with NDWI and a relatively strong correlation with NDBI. This study observes a consistent increase in LST on built-up land, which impacts surrounding land uses. This trend suggests that the urban heat island effect will likely persist in the CMA in the future. To mitigate the effects of rising temperatures, this study recommends increasing green spaces, regulating and monitoring new constructions, creating more green infrastructure, and protecting water bodies. These measures may help reduce LST and promote sustainability in the region.

References

Anushiya J., Ramachandran, A., & Palanivelu, K. (2021). Challenges in Chennai City to cope with changing climate. *European Journal of Climate Change*, 3(1), 33-43.

Ayanlade, A., Aigbiremolen, M. I., & Oladosu, O. R. (2021). Variations in urban land surface temperature intensity over four cities in different ecological zones. *Scientific Reports*, 11(1), 20537.

Chanu, C. S., Elango, L., & Shankar, G. R. (2021). A geospatial approach for assessing the relation between changing land use/land cover and environmental parameters including land surface temperature of Chennai metropolitan

city, India. *Arabian Journal of Geosciences*, 14, 1-16.

Chatterjee, U., & Majumdar, S. (2022). Impact of land use change and rapid urbanization on urban heat island in Kolkata city: A remote sensing based perspective. *Journal of Urban Management*, 11(1), 59-71.

Chen, Y., Yang, J., Yu, W., Ren, J., Xiao, X., & Xia, J. C. (2023). Relationship between urban spatial form and seasonal land surface temperature under different grid scales. *Sustainable Cities and Society*, 89, 104374.

Cohen, J. (1960). A coefficient of agreement for nominal scales. Educational and psychological measurement, 20(1), 37-46.

Das, T., & Das, S. (2022). Analysing the role of land use and land cover changes in increasing urban heat phenomenon in Chandannagar city, West Bengal, India. *Journal of Earth System Science*, 131(4), 261.

Foody, G. M., & Mathur, A. (2004). A relative evaluation of multiclass image classification by support vector machines. *IEEE Transactions on geoscience and remote sensing*, 42(6), 1335-1343.

Ghobadi, Y., Pradhan, B., Shafri, H. Z. M., & Kabiri, K. (2015). Assessment of spatial relationship between land surface temperature and landuse/cover retrieval from multi-temporal remote sensing data in South Karkheh Sub-basin, Iran. *Arabian Journal of Geosciences, 8*, 525-537.

Hansen, J., Ruedy, R., Sato, M., & Lo, K. (2010). Global surface temperature change. *Reviews of Geophysics*, 48(4).

Kesavan, R., Muthian, M., Sudalaimuthu, K., Sundarsingh, S., & Krishnan, S. (2021). ARIMA modeling for forecasting land surface temperature and determination of urban heat island using remote sensing techniques for Chennai city, India. *Arabian Journal of Geosciences*, 14(11), 1016.

Krishnamurthy, R., & Desouza, K. C. (2015). Chennai, India. *Cities, 42*, 118-129.

Mishra, V. N., Prasad, R., Rai, P. K., Vishwakarma, A. K., & Arora, A. (2019). Performance evaluation of textural features in improving land use/land cover classification accuracy of heterogeneous landscape using multi-sensor remote sensing data. *Earth Science Informatics*, 12, 71-86.

Openshaw, S. (1996). Developing GIS-relevant zone-based spatial analysis methods. *Spatial analysis: modelling in a GIS environment*, 55-73.

Prestele, R., Alexander, P., Rounsevell, M. D., Arneth, A., Calvin, K., Doelman, J. & Verburg, P. H. (2016). Hotspots of uncertainty in land-use and land-cover change projections: a global-scale model comparison. *Global change biology*, 22(12), 3967-3983.

Saha, P., Bandopadhyay, S., Kumar, C., & Mitra, C. (2020). Multi-approach synergic investigation between land surface temperature and land-use land-cover. *Journal of Earth System Science*, 129, 1-21.

Shahfahad, Kumari, B., Tayyab, M., Ahmed, I. A., Baig, M. R. I., Khan, M. F. & Rahman, A. (2020). Longitudinal study of land surface temperature (LST) using mono-and split-window algorithms and its relationship with NDVI and NDBI over selected metro cities of India. *Arabian Journal of Geosciences*, 13, 1-19.

Singh, P., Rana, P. J. S., Mukherjee, R., & Srivastava, P. (2018). A step towards environmental benign Mg/Pb based binary metal mixed halide perovskite material. *Solar Energy*, 170, 769-779.

Singh, S. K., Srivastava, P. K., Gupta, M., Thakur, J. K., & Mukherjee, S. (2014). Appraisal of land use/land cover of mangrove forest ecosystem using support vector machine. *Environmental Earth Sciences*, 71(5), 2245-2255.

Sun, Q., Wu, Z., & Tan, J. (2012). The relationship between land surface temperature and land use/land cover in Guangzhou, China. *Environmental Earth Sciences*, 65, 1687-1694.

Sun, Y., Wang, Z., Fu, P., Jiang, Q., Yang, T., Li, J., & Ge, X. (2013). The impact of relative humidity on aerosol composition and evolution processes during wintertime in Beijing, China. *Atmospheric Environment*, 77, 927-934.

Tang, B. H., Wu, H., Li, C., & Li, Z. L. (2011). Estimation of broadband surface emissivity from narrowband emissivities. *Optics Express*, 19(1), 185-192.

Vapnik, V. (1995). *Statistical Learning Theory*, New York, NY: Springer-Verlag, 736.

Verburg, P. H., Crossman, N., Ellis, E. C., Heinimann, A., Hostert, P., Mertz, O., Nagendra, H., Sikor, T., Erb, K. H., Golubiewski, N., Grau, R., Grove, M., Konaté, S., Meyfroidt, P., Parker, D. C., Chowdhury, R. R., Shibata , H., Thomson , A. & Zhen, L. (2015). Land system science and sustainable development of the earth system: A global land project perspective. *Anthropocene*, 12, 29-41.

Verma, P., Raghubanshi, A., Srivastava, P. K., & Raghubanshi, A. S. (2020). Appraisal of kappa-based metrics and disagreement indices of accuracy assessment for parametric and nonparametric techniques used in LULC classification and change detection. *Modeling Earth Systems and Environment*, 6, 1045-1059.

Yang, J., Wang, Z. H., & Kaloush, K. E. (2015). Environmental impacts of reflective materials: Is high albedo a 'silver bullet' for mitigating urban heat island?. *Renewable and sustainable energy reviews*, 47, 830-843.

Yin, C. L., Meng, F., & Yu, Q. R. (2020). Calculation of land surface emissivity and retrieval of land surface temperature based on a spectral mixing model. *Infrared Physics & Technology*, 108, 103333.

Manikandan N.*
Guest Lecturer,
Department of Geography,
School of Earth and Atmospheric Sciences.
University of Madras,
Guindy Campus, Chennai, Tamilnadu

Dharshan Shylesh D. S.
Research Scholar,
Department of Geography,
University of Madras,
Guindy Campus, Chennai, Tamilnadu

Jaganathan R.
Professor and Head,
Department of Geography,
University of Madras,
Guindy Campus, Chennai, Tamilnadu

Mahalingam B,
Assistant Professor,
Department of Geography,
School of Earth Sciences,
Central University of Karnataka,
Kadaganchi, Kalaburagi, Karnataka

Sivasankar S.
Faculty Member,
Department of Geography,
University of Madras,
Guindy Campus, Chennai, Tamilnadu

Sangunathan U.
Project Associate,
Environmental and Water Resources Engineering (EWRE) Division,
Department of Civil Engineering,
Indian Institute of Technology Madras,
Guindy, Chennai, Tamilnadu

Manivel P.
Guest Lecturer,
Department of Geography,
School of Earth and Atmospheric Sciences.
University of Madras,
Guindy Campus, Chennai, Tamilnadu

*Author for Correspondence
E-mail: maninresearcher@gmail.com